Journal of Laser Applications ARTICLE pubs.aip.org/lia/jla

X-ray analysis of capillary and melt pool dynamics using laser beam oscillation welding for aluminum die-casts

Cite as: J. Laser Appl. **37**, 022019 (2025); doi: 10.2351/7.0001639
Submitted: 15 July 2024 · Accepted: 20 March 2025 ·
Published Online: 8 April 2025

Stephan Börner,[1,a)] Dirk Dittrich,[1] Tim Sahm,[1] Linda Ullmann,[1] Paul Hans Kamm,[2] and Axel Jahn[1]

AFFILIATIONS

[1]Fraunhofer Institute for Material and Beam Technology IWS, Winterbergstr. 28, Dresden 01277, Germany
[2]Helmholtz-Zentrum Berlin fuer Materialien und Energie, Hahn-Meitner-Platz 1, Berlin 14109, Germany

Note: Paper published as part of the special topic on Proceedings of the International Congress of Applications of Lasers & Electro-Optics 2024.

[a)]**Author to whom correspondence should be addressed:** stephan.boerner@iws.fraunhofer.de

ABSTRACT

The knowledge of underlying physical phenomena and the understanding of parameter dependencies are essential for the development of stable welding processes. Quantitative data based on a sensor-based approach are necessary to draw conclusions about the resulting quality. These are at the same time key factors for the optimization of industrial processes. The paper refers to this in the context of laser welding technology using superimposed dynamic beam oscillation of aluminum alloys. However, particularly die-cast aluminum is characterized by limited weldability due to entrapped gases, which lead to defects like high porosity and blow out formation along the weld seam. For the welding trails, a novel laser processing head was designed. The optics enables a synchronized and fast beam deflection in all three spatial directions. Therefore, a galvanometer scanner for x-y-oscillation was combined with a piezo-driven mirror for the beam movement in the z-direction. By means of *in situ* synchrotron x-ray imaging synchronized with recordings of acoustic process emissions and high-speed imaging of the melt pool, deep insights into the interactions of the laser beam and material could be investigated. The collected data show a clear correlation between oscillation parameters (frequency and amplitude) and the resulting weld seam quality. Furthermore, audio signal information provides an explicit link for different vapor capillary formations as well as melt flow fluctuations. The adapted process dynamics for dynamic beam oscillation welding enable a significant quality improvement and open up the possibility for efficient and safe process monitoring.

Key words: laser beam welding, laser scanning, x-ray imaging, acoustics, capillary waves, aluminum, solidification process, porous media, optical imaging, synchrotron radiation

I. INTRODUCTION

A specific challenge in laser welding applications of aluminum alloys is pore formation. Different mechanisms have been reported that can lead to those irregularities. One of the main causes is the solubility of hydrogen and other gases in aluminum, which is temperature dependent and dramatically increases in the molten phase. On the other hand, contaminations or inclusions in the material as well as keyhole phenomena like strong fluctuations and constriction of the keyhole during the process can cause high porosity.[1–6]

Figure 1 shows a transmission image with crater formation and high porosity as typical weld defects during laser welding of aluminum die-cast materials.

It is already known from the literature that superimposed beam oscillation can have a positive effect on the laser welding process due to the stabilization of the keyhole and reduction of defects. In recent years, the laser welding process has been increasingly accurately described through the analysis of *in situ* x-ray images and simulations. This paper aims to contribute to the understanding of the mechanisms of different oscillation regimes by

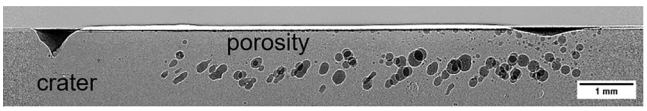

FIG. 1. Typical weld seam defects for aluminum die-cast laser welding with crater formation and high porosity in x-ray transmission image.

analyzing selected x-ray recordings of laser welded aluminum die-casting. The goal is to facilitate the selection of oscillation parameters for high-quality welding results. Additionally, it aims to investigate whether conclusions about seam quality can be drawn from the acoustic emissions of the laser welding process.

II. STATE OF THE ART

A. Laser welding of aluminum die-cast

Aluminum die-casting is a material that is difficult to weld because it tends to form pores and melt ejections can occur due to inclusions in the material. This can critically impact component properties such as strength and tightness. Laser welding, as a flexible and highly automated process, is ideally suited to achieve high quality requirements. Since a multitude of the aforementioned seam defects can occur with classical static welding, various approaches have been pursued to improve process stability and seam quality (Fig. 2). In addition to laser-based procedures, other joining technologies of aluminum such as friction stir welding, arc welding, and mechanical joining methods have been described that are beyond the scope of this report.

The laser-based methods can be divided into two groups. On the one hand, approaches have been pursued in which the seam quality was improved by adjusting the ambient conditions during laser welding. One possibility is laser welding under reduced ambient pressure or vacuum. In Ref. 7, it was shown that in a vacuum, both the penetration depth increases and spatter and the vapor plume can be reduced. Additionally, a significant influence of the base material on the welding result was observed. The results from Ref. 8 show that using an electromagnetic field can reduce porosity and lead to a smooth seam surface. Another approach is the use of sound wave excitation, which was examined in Ref. 9 and used to influence the melt pool.

On the other hand, there are approaches in the literature where the energy input of the laser beam itself has been adjusted for process optimization. By using high welding speeds, for example, a reduction of porosity was achieved in Refs. 10 and 11. In Ref. 12 the use of a multispot optic and beam shaping stabilized the keyhole, thereby reducing the resulting pore volume. Sokolov *et al.*[13] found in their studies that a balanced energy input through the combination of dual-laser beam and frequency beam oscillation can lead to an improvement in seam quality. The use of beam oscillation with a single mode laser showed a significant improvement in seam quality.[14] By repeatedly passing over, cavities in the base material and bubbles in the melt pool can be gradually degassed. By maintaining a stable vapor capillary during high-frequency laser welding, process pores and melt ejections were minimized,[15] resulting in pressure-tight components.

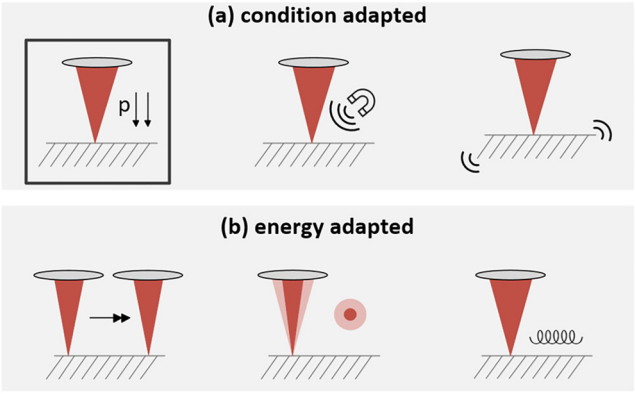

FIG. 2. Overview of laser welding approaches of aluminum die-cast grouped in (a) condition adapted (reduced ambient pressure, sound wave excitation, electromagnetic field) and (b) energy adapted (high welding speed, beam shaping, beam oscillation).

B. Process monitoring for laser welding

The quality of a weld joint is a crucial factor for the further use of the components. To ensure reliable and consistent quality of the weld joints, monitoring the process stability in production is advisable. During laser welding, different process emissions are generated, which can be used for process monitoring (Fig. 3).

The electromagnetic emissions, such as the reflected laser radiation, the thermal radiation from the melt, or the emissions from the metal vapor, can be detected using camera-based systems or photodiodes.[17,18] Other widely used methods are the use of optical coherence tomography for monitoring the penetration depth or post-process observation with triangulation principle-based sensors for the weld seam shape.[19,20]

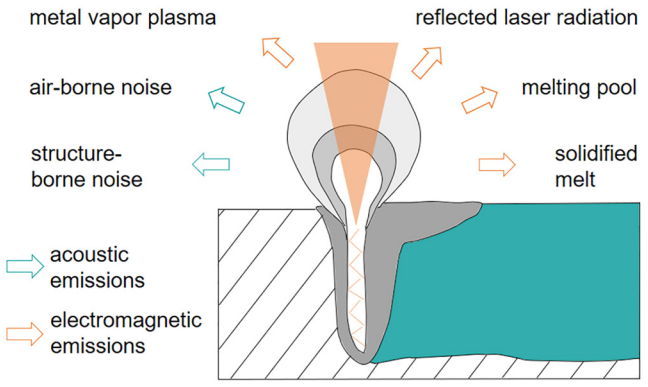

FIG. 3. Process emissions during keyhole laser welding according to Refs. 16 and 17.

Additionally, various acoustic emissions are emitted during the process, which can be recorded using, e.g., structure-borne sound sensors or microphones. Based on this approach, Luo *et al.*[21] described the influence of keyhole geometry on the acoustic signals emitted during welding. However, these studies on laser welding concentrated on lower-frequency acoustic airborne noise emissions. Due to the high temporal resolution of current devices, the use of acoustic emissions shows great potential for capturing the frequently occurring high temporal fluctuations of the laser welding process.

III. METHODS

A. Laser equipment

For the welding experiments, a combination of a 2 kW single-mode laser from IPG Photonics with a specifically developed 3D scanner was used. The processing head consists of a classic X-Y scanner (welDYNA from Scanlab), in conjunction with a piezoelectric mirror (Zwobbel®-1020 from RobustAO) for additional oscillation of the beam in the z-direction. The specifications of the laser equipment can be found in Tables I and II.

In addition to the mechanical integration of the z-mirror on a classical scanner, calibration of the system, including synchronization of the axes, is necessary to utilize the system for expanding the parameter space for process influence in industrial applications. Nevertheless, the costs are affordable for small and medium-sized enterprises (SMEs) compared to other intensity modulation tools.

For synchronized beam movement in all three spatial directions, it is crucial to use one control unit. For this purpose, the ESL-2-100 module developed at Fraunhofer IWS was used, which allows for the adjustment of frequencies f and amplitudes a as well as phase shift for all three axes. With the 3D scanner used, it is possible to alter the beam's path in the X–Y plane and along the propagation axis, creating further possibilities for adjusting energy distribution (Fig. 4). Additionally, it allows for targeted adjustment of the focal position without an additional machine axis, enabling, e.g., efficient welding of 3D contours.[22]

The experimental setup, which was installed into the TOMCAT beamline at the Swiss Light Source (SLS) at Paul Scherrer Institut (PSI) in Villigen (CH), is depicted in Fig. 5. The relative movement between the laser beam and the workpiece was enabled by the additionally integrated linear axis. Using the stationary processing head, only the beam oscillation in the various spatial directions was realized. Argon with a flow rate of 10 l/min was used as the shielding gas. The cross jet protected the optics from contamination with spatter and metal vapors. The sensors used remained stationary during the experiments and were aligned with the corresponding process zone.

TABLE I. Specification of used beam source and optics.

Laser source	YLS-2000-SM
Maximum laser power	2000 W
Wavelength	1070 nm
Beam parameter product	0.4 mm mrad
Core fiber diameter	30 μm
Magnification	1:1.25

TABLE II. Specification of the used 3D processing head.

Device	welDYNA	Zwobbel®-1020
Osc. direction	X and Y	Z
Max. osc. frequency	4000 Hz	500 Hz
Max. osc. amplitude	0.4 mm	11.5 mm

B. Process observation tools

To better understand the causes of the irregularities and to develop potential solutions, a combination of various observation tools was used in the measurement series. In addition to a conventional high-speed camera, a laser-optical microphone was integrated into the x-ray setup. Selected specifications and the recording rates are listed in Table III.

For the analysis of melt pool behavior and keyhole movements from the outside, a high-speed XS Mini HD camera from IDT Inc. with corresponding LED lighting was used. With a recording rate of 10 000 Hz, it was also possible to detect spatter and melt ejections during the welding process.

The intense polychromatic synchrotron x-ray radiation of the 2.9 T bending magnet at the TOMCAT beamline was filtered with 1.45 mm Si and converted to visible light using a 150 μm-thick LuAG:Ce scintillator. Images were acquired at a rate of 5000 Hz with the GigaFRoST camera system at a 4× magnification, resulting in an effective pixel size of 2.75 μm.[23,24]

The use of synchrotron x-ray radiation enabled an in-depth insight into the interaction of the laser beam with the bulk material. The main focus here was on the analysis of pore formation, the development of the vapor capillary, as well as the melt pool and the corresponding flows within. In addition to the *in situ* measurement, an image of the initial state and the final state of the sample was taken. Therefore, longitudinal transmission images of the sample before and after welding were taken and combined using the ImageJ plugin Grid/Collection Stitching. This allows both the porosity of the welded sample to be analyzed and correlations to be drawn regarding seam quality, for example, in relation to the initial state.

To capture the acoustic process emissions, a laser-optical microphone (Eta250 Ultra, XARION Laser Acoustics) was used. The measurement principle is based on the Fabry-Pérot interferometer

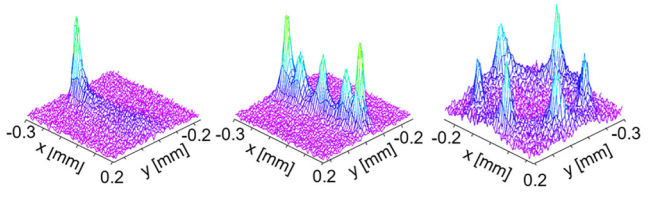

FIG. 4. Selection of measured intensity profiles, which are possible with specially developed 3D-beam oscillation processing head.

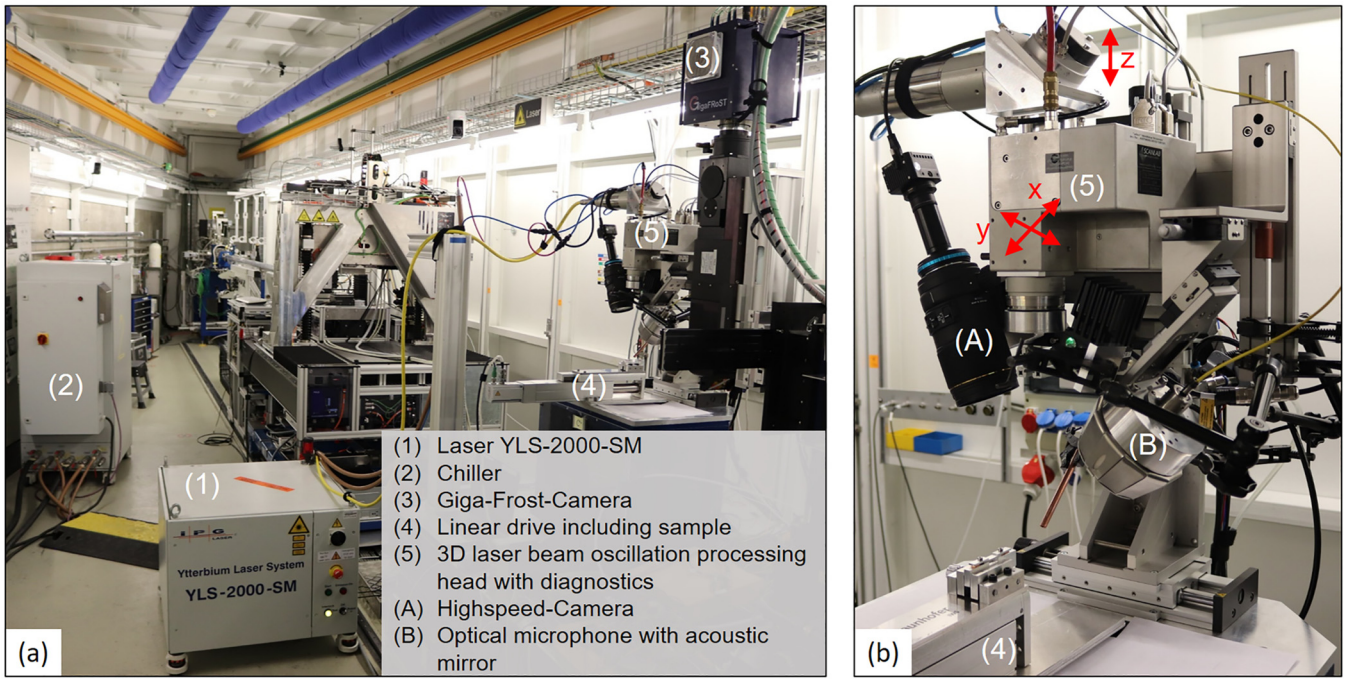

FIG. 5. Experimental setup integrated into TOMCAT beamline at the SLS at PSI, Villigen (CH), (a) overview of the setup and (b) detailed view of the processing head and process diagnostics. For beam oscillation in 3D space, a piezo-driven mirror (for z-direction) was combined with a galvanometer scanner (for x,y-direction).

and is described in detail and mathematically derived in the patents WO 2008/000007 and WO 2012/163681 A1. To specifically amplify the acoustic process emissions to be captured, an acoustic elliptical mirror was designed and used. The elliptical mirror uses the shape of an ellipse defined by two focal points. Rays originating from one focal point are reflected to the other. One of the focal points is located in the process zone, while the microphone is positioned at the other.

C. Material

For the experiments, two typical aluminum die-casting alloys, AC-AlSi9MnMoZr and AC-AlSi10MnMg, were used. The nominal chemical composition of those materials is summarized in Table IV. For the welding trials plates with a thickness of 3 mm were used, which were produced in an atmospheric die-casting process. Samples with dimensions of $60 \times 20\ \text{mm}^2$ were cut out from them. Traditional die-casting is characterized by its high production efficiency and good surface finish.[25] However, particular challenges during welding are inclusions in the material such as release agents, gases, or other contaminants that may remain in the material during the rapid cooling in the manufacturing process. Three trials of penetration welding were performed on the middle axis of the narrow sample side with a distance of 7.5 mm between the seams and the edges. The weld seam length was set to 10 mm.

D. Experimental plan

Initial investigations by Börner *et al.*[26] demonstrate the influence of oscillation parameters on weld seam quality. This contribution aims to closely examine the relationship between beam path speed and weld seam quality and derive the effects on melt pool and keyhole formation. For this purpose, welds were performed with variations in oscillation frequency between 250 and 4000 Hz

TABLE III. Specification of the used diagnostics.

Sensor	Optical	X-ray	Audio
Name	XS Mini HD Cam	GigaFroST	Eta250 Ultra
Company	IDT Inc	PSI	Xarion LA
Resolution	7.46 μm/Px	2.75 μm/Px	$10–1 \times 10^6$ Hz
Sampling rate	10 000 Hz	5 000 Hz	2 000 000 Hz

TABLE IV. Nominal chemical composition of the investigated materials.

	Chemical composition in wt. %					
Material	Al	Si	Fe	Cu	Mn	Mg
AC-AlSi9 MnMoZr	Bal.	10.5	0.15	0.05	0.6	0.06
AC-AlSi10 MnMg	Bal.	11.5	0.15	0.03	0.8	0.5

at identical energy per unit length of 15 J/mm and constant amplitudes of 0.2 mm on the two aforementioned die-casting alloys. Reference welds with static beam guidance were produced for comparison. Furthermore, initial trials with the novel beam oscillation head were performed to determine opportunities for melt pool and capillary shaping by x-z-oscillation. Additionally, the acoustic process emissions were to be analyzed in more detail to draw conclusions about the weld seam quality from the audio signals.

IV. RESULTS AND DISCUSSION

A challenge in welding is the formation of pores, especially in aluminum alloys. Particularly for aluminum die-casts, pore formation is well documented in the literature, making it very difficult to weld.

A. Influence of beam oscillation frequency on weld seam quality

The results of the test series show a strong dependence of weld quality on the welding parameters used for laser welding of two classic die-casting alloys (AC-AlSi9MnMoZr and AC-AlSi10MnMg). In Figs. 6 and 7, longitudinal transmission images of the samples are juxtaposed, where a welding depth of approximately 1 mm was targeted with a constant energy per unit length of 15 J/mm. The images shown are the results of a division between the initial state and the final state. The pores formed during welding are depicted in black. The white cavities are inclusions in the initial state, which have been welded-over and were affected by the welding process. This allows conclusions to be drawn about the influence of the initial state.

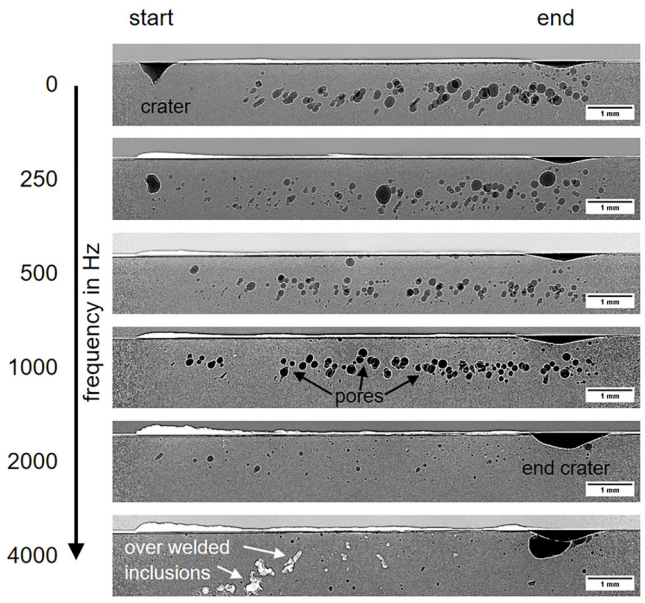

FIG. 6. Longitudinal transmission images of weld seams for AC-AlSi9MnMoZr. Influence of beam oscillation frequency on weld seam quality.

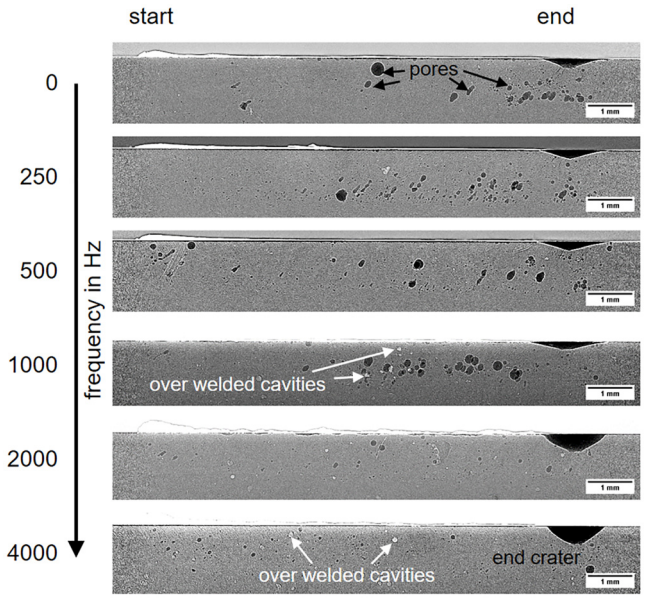

FIG. 7. Longitudinal transmission images of weld seams for AC-AlSi10MnMg. Influence of beam oscillation frequency on weld seam quality.

1. Laser welding of AC-AlSi9MnMoZr

The test results for the material AC-AlSi9MnMoZr in Fig. 6 show a clear influence of welding parameters on the resulting seam quality.

The statically welded seam ($f_{x,y} = 0$ Hz) exhibits the highest porosity of all samples. Additionally, a crater is visible at the beginning of the seam, which was created when piercing the cavity and the resultant ejection of the melt. The resulting pores tend to have an elongated shape. These can be attributed to the mechanism of bubbles adhering to the solidification front in the melt pool, forming elongated pores.[5]

When using superimposed beam oscillation, different welding results are achieved depending on the frequency range. At lower beam oscillation frequencies up to 1000 Hz, a similar picture emerges as in the static experiment, with comparatively high porosity and pore sizes up to a diameter of 320 μm. However, in the welds with 2000 and 4000 Hz, a drastic reduction in porosity is evident. Particularly noteworthy is the result with the highest frequency, where various inclusions in the first half of the weld seam (depicted in white in the image) were welded over and had no significant impact on pore formation, and no ejection occurred, as confirmed by the high-speed recordings of the experiment.

Additionally, various trends related to oscillation frequency can be derived from the test series. It becomes apparent that the size of the end crater tends to increase with the oscillation frequency used, and there is an accumulation of material or an elevated seam at the beginning of the weld seam. In the seam welded with $f_{x,y} = 4000$ Hz, a bubble that is just degassing can also be discerned, which remained in the material due to the progressive solidification process after the laser beam is switched off. Conversely,

it is observed that the majority of pores are located in the lower part of the seam (from about 0.5 mm) and only a few pores appear in the upper part of the seam. The causes of these results will be discussed in more detail later.

2. Laser welding of AC-AlSi10MnMg

In the test series with the material AC-AlSi10MnMg, the weld seam produced with static beam guidance also exhibits high porosity (see Fig. 7). In contrast, the experiments with superimposed beam oscillation show that pore formation can be significantly reduced in some cases. With increasing frequency, a reduction in porosity becomes evident.

Notably, the welding with $f_{x,y} = 1000$ Hz deviates from this trend. The cause of this deviation is inclusions within the base material, which are visible as white cavities in the middle of the seam. From this region, there is a significant accumulation of pores. Despite individual cavities in the initial state in the samples with 2000 and 4000 Hz, the porosity is very low.

For the AC-AlSi10MnMg samples, a similar trend to the AC-AlSi9MnMoZr samples is observed, with an increase in end crater size with oscillation frequency and comparable pore formation in terms of shape. At frequencies up to 500 Hz, the proportion of elongated pores is larger than at higher frequencies. Regarding pore distribution, no clear correlation of oscillation frequency can be drawn, although many pores tend to form in the lower part of the weld seam.

B. *In situ* observation of welding phenomena during beam oscillation welding

Section IV B examines the causes of the different seam qualities, particularly with regard to pore formation, using the x-ray images. For this purpose, characteristic process sequences will be compared for the samples made from AC-AlSi10MnMg, and several process phenomena during welding will be explained.

1. Classical laser beam oscillation welding

In the x-ray images in Fig. 8 for the experiment with $f_{x,y} = 1000$ Hz, an oscillating keyhole with a diameter of approximately 55 μm and a depth between 630 and 960 μm, pending on the position, can be seen, which moves along its circular path. During the welding process, bubbles occasionally become visible in the melt pool, likely caused by trapped gases in the base material. Some bubbles can be degassed by multiple passes of the keyhole. This phenomenon is already known from the literature.[5,27]

In the presented sequence, a piercing process of a cavity is illustrated, which leads to the generation of a bubble with a diameter of approximately 280 μm. This bubble moves through the melt pool due to the melt flow caused by the oscillating keyhole. In the sequence, there is no interaction of the keyhole with the bubble visible. 2 ms after the piercing process, the bubble settles down at the solidification front and grows into a pore due to lower melt flow in the rear section of the melt pool. In the last image of the sequence, another start of a piercing process becomes obvious.

As the process progresses, the process zone encounters the piercing of trapped cavities. This leads to significant process

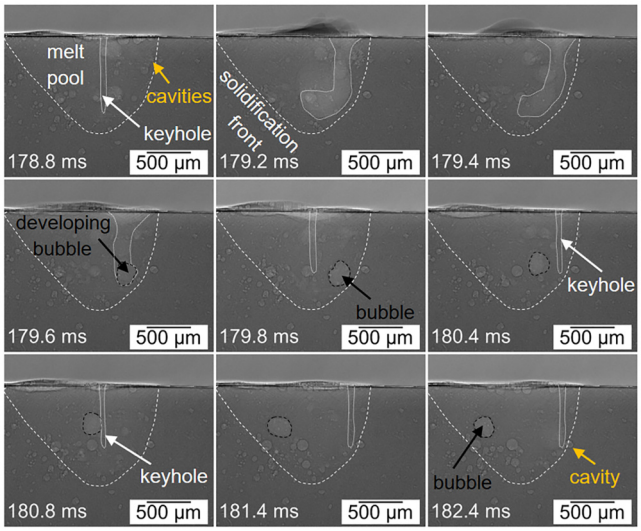

FIG. 8. Sequence of *in situ* x-ray recordings for beam oscillation welding of AC-AlSi10MnMg with low frequency ($f = 1000$ Hz). Piercing of gas cavities (marked with red) resulting in high porosity.

fluctuations and an accumulation of these fluctuations, ultimately resulting in substantial pore formation. Even with multiple passes, the bubbles cannot be completely degassed and remain in the material due to the progressing solidification.

2. Dynamic laser beam oscillation welding

For welding at $f_{x,y} = 4000$ Hz, there is a regime change compared to the classical beam oscillation at lower frequencies. The x-ray images in Fig. 9 show that there is a widening of the vapor capillary and a change in the melt pool shape as well as the flow conditions. The widening of the capillary is probably due to the high relative speed of the beam and the comparatively small process interaction zone with simultaneously high intensity. The width of the vapor channel fluctuates greatly during the process. At the half length of the capillary, the diameter varies by 300 μm. For the opening of the capillary on the surface, a width between 1.05 and 1.25 mm can be determined.

The strong fluctuations of the capillary have a positive effect on the behavior of the melt pool. On the surface, waves form in the rear part of the melt pool. This leads to stronger flows from the surface along the solidification front toward the capillary. Bubbles formed in the melt pool can thus be moved near the capillary and degassed more easily there. It is additionally pertinent to mention that the solidification front is steeper than in the process with classical beam oscillation (compare Fig. 8).

The procedure starting from piercing of a cavity to the final degassing of the bubble is visualized in the sequence in Fig. 9. Due to the larger vapor channel, bubbles can be degassed faster on the one hand, and process fluctuations do not affect the capillary as much on the other. The probability of a capillary narrowing and a collapse is also reduced. The enlarged end crater, visible in Fig. 7 for

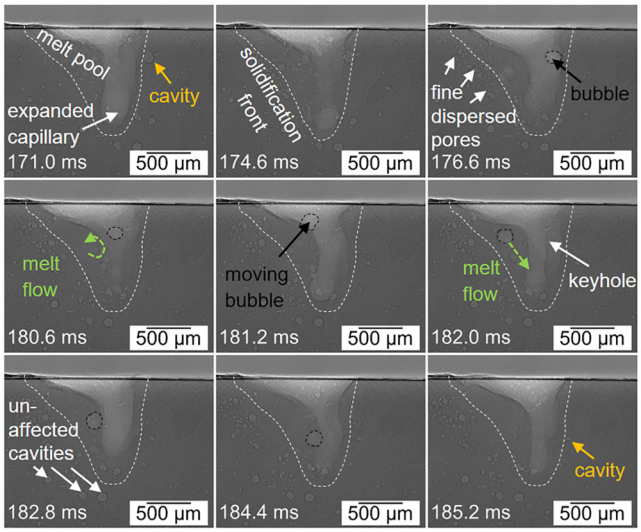

FIG. 9. Sequence of *in situ* x-ray recordings for beam oscillation welding of AC-AlSi10MnMg with high frequency ($f = 4000$ Hz). Piercing of gas cavities (marked with red) and degassing of bubbles by the expanded vapor capillary and melt flow change.

welding at $f_{x,y} = 4000$ Hz, can also be attributed to the significantly larger capillary.

C. Acoustic sensor for process monitoring

Section IV C presents the results of the additional acoustic measurements and explores the possibilities of using a laser-optical microphone for process monitoring.

1 . Comparison of different process regimes

In addition to the quality of the welds, differences are also evident in the audio signal recorded during the experiments (Fig. 10). The figure visualizes the audio signals of the XARION Eta250 microphone as a spectrogram for the locally oscillating keyhole and the process regime with an expanded vapor capillary. There is a significant increase in the sound pressure level at the beginning of the welding process and a decrease when the laser beam was turned off.

For the welding trial with a beam oscillation frequency of 4000 Hz, higher signal intensity in a wide frequency range can be observed compared to the welding process with a lower beam oscillation frequency. Particularly for frequencies in the range of 100–500 kHz, larger amplitudes can be determined for experiments with an expanded capillary. This can likely be attributed to the expansion of the vapor capillary, thereby increasing the size of the resonance body. Additionally, significantly larger fluctuations in the melt pool and capillary walls were observed in the x-ray images.

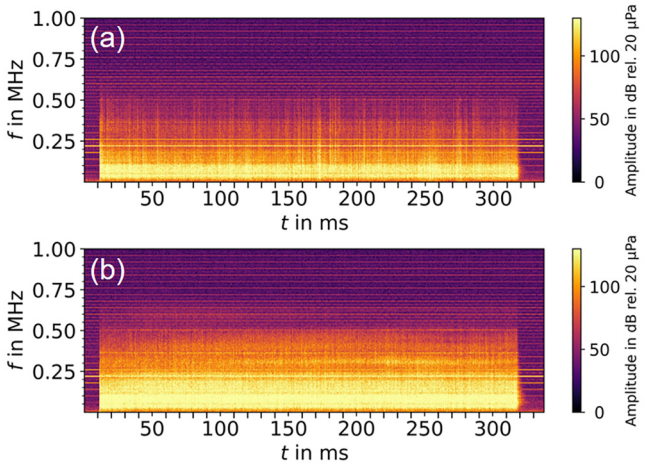

FIG. 10. Audio signals for welding process with (a) local oscillated keyhole and (b) expanded capillary. Trials were performed without using cross jet to detect a clear audio signal from the welding process.

2. Detection of process irregularities

An important aspect of targeted process monitoring is ensuring that the system functions under real production conditions. In the subsequent experiments, realistic boundary conditions were tested and the cross jet was activated to verify whether the welding process signal stands out sufficiently from the ambient noise. Therefore, the use of the acoustic mirror particularly amplifies the signal in the process zone.

Another crucial point in the use of process monitoring tools is the detection of process irregularities. A parameter was chosen for this purpose that lies in the transition region between a locally oscillating keyhole and an expanded vapor capillary. In the x-ray images from the *in situ* measurement in Fig. 11(a), a regime change during a process is demonstrated.

At the beginning, an expanded capillary can be observed. At the time of 120 ms, the regime changes, and only a locally oscillating keyhole becomes visible. This is also reflected in the audio signal in Fig. 11(b). Initially, larger signal amplitudes are observed in the frequency range above 100 kHz, and after 120 ms, the amplitudes generally flatten out in this range. The longitudinal section in Fig. 11(c) also shows different welding results, with lower porosity for the expanded capillary and an increase in pore formation in the section with the local oscillated keyhole.

3. Opportunity for repair

To operate a resource-efficient production, it is important to recognize these differences and take appropriate measures after a detailed analysis of the component and the causes of defects. One option is to re-weld the seam with an adjusted parameter set, as visualized in Fig. 12.

It is additionally pertinent to mention that the width of the melt pool, which is smaller for the re-welding process compared to the original weld seam, leads to different weld seam widths.

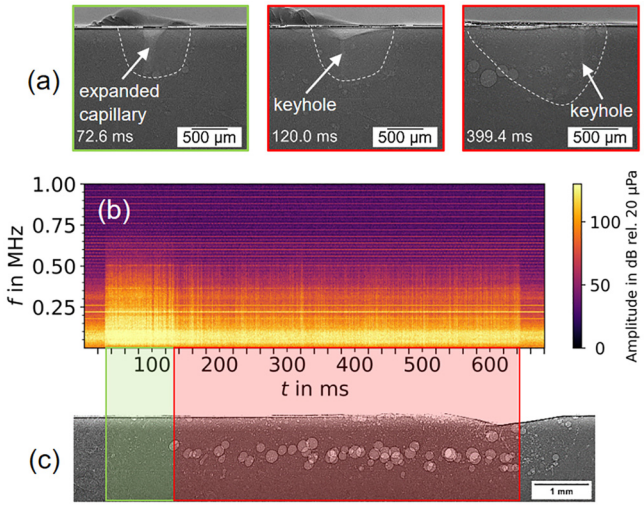

FIG. 11. Welding trial with regime change from expanded capillary to oscillated keyhole (a) excerpts of the *in situ* x-ray recordings, (b) audio signal, and (c) longitudinal transmission image of after welding state.

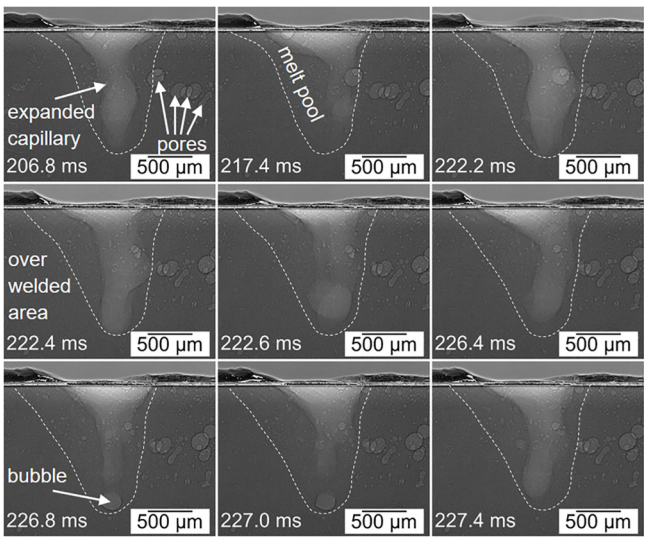

FIG. 13. Sequence of re-welding process with degassing of pores by expanded capillary.

Through the expanded capillary and the change in melt pool flow, it is possible to degas a large portion of the resulting pores during re-welding (Fig. 13). A stable capillary is visible during over-welding. Bubbles that appear can degas through the expanded degassing channel. The comparison with Fig. 11 shows that the quality of the result has improved significantly.

Due to the differences in the seam widths, the re-welding process can not affect all pores and a few pores remain in the sample after the process [Fig. 14(b)]. Thereby, both the x-ray image and the audio signal in Fig. 14(a) indicate that welding was consistently performed with an expanded capillary.

The results show that targeted adjustment of the melt pool shape and keyhole formation can positively influence the seam quality. Additionally, it is possible to detect these quality differences indirectly through the audio signals and initiate appropriate further steps.

D. Transfer to novel beam oscillation

Another way to influence the melt pool and keyhole formation is to extend the oscillation movement along the beam propagation z-axis. Section IV D illustrates the initial results in this regard. Additionally, the analysis of acoustic emissions for process monitoring will be continued.

1. X-ray analysis

Figure 15 shows a sequence of x-ray images of a welding process with x-z-oscillation. By oscillating the beam in the z-direction, the focal point can be shifted both above and into the specimen. This alters the intensity of the beam on the surface due to beam caustics, which in turn affects the formation of the vapor capillary. By additionally oscillating in the x-direction, different beam intensities can be generated in the feed direction, thereby influencing the melt pool.

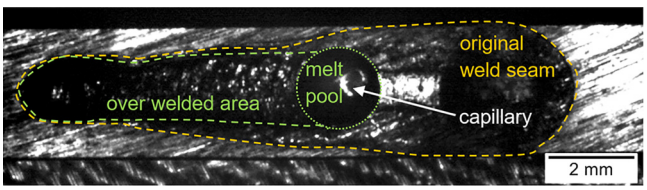

FIG. 12. Comparison of weld seam width and melt pool size extracted from high speed imaging of re-welding process from the top of the sample.

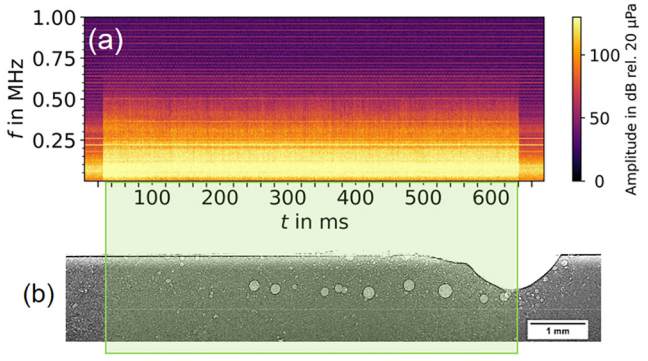

FIG. 14. (a) Audio signal for repair welding process and (b) longitudinal transmission image of final state after over welding with significant porosity reduction.

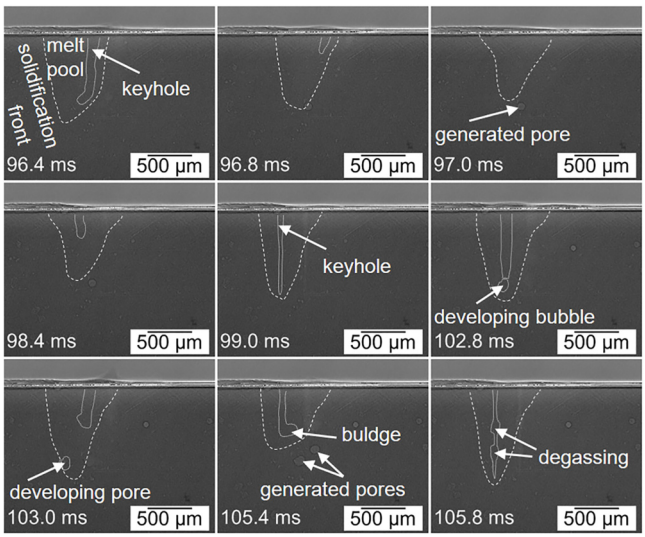

FIG. 15. Sequence of an x-z-oscillation welding process with bubble generation due to the separation of the keyhole root, keyhole shaping, and degassing of bubbles in the melt pool.

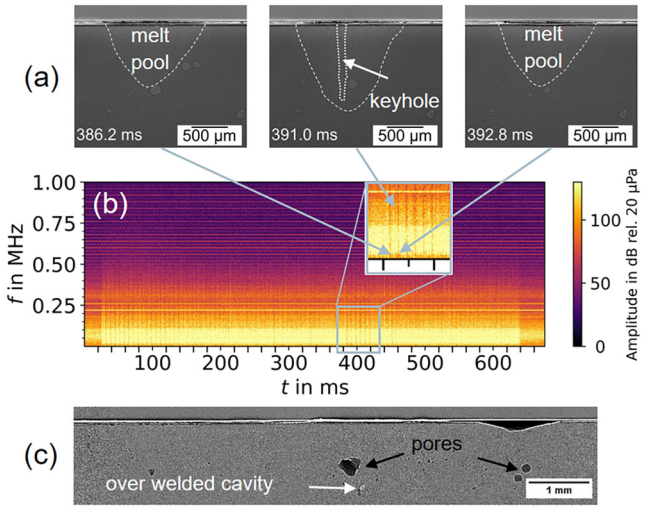

FIG. 16. (a) Excerpts of *in situ* x-ray recordings, (b) audio signal, and (c) longitudinal transmission image for a welding process with x-z-oscillation.

The vapor capillary oscillates in the feed direction due to the set x-oscillation at $f_x = 300$ Hz and $a_x = 0.3$ mm. The superimposed oscillation of the beam in the z-direction leads to a change in the keyhole size as well as the melt pool shape according to the oscillation frequency in the z-direction of 150 Hz. The phase shift between the oscillation axes was chosen so that the intensity peak at the surface is at the rear of the melt pool, creating a narrow keyhole in this area and only a shallow keyhole depth in the front area of the melt pool.

In the presented sequence, the keyhole depth fluctuates between 880 μm at the rear position and 176 μm at the melt pool front. Moreover, at the front position, the keyhole disappears at 97.0 ms and becomes visible again after 1.4 ms. This is probably caused due to low intensity on surface at the front reversal point during the x-z-oscillation and is repeated with a frequency of 150 Hz.

The sequence also shows the degassing of a bubble by re-passing the keyhole (see Fig. 15 at 99 ms). The other part of the sequence beginning from 102.8 ms is intended to visualize the generation of bubbles in the melt pool due to a separation of the keyhole root and the degassing of those bubbles by re-passing of the keyhole.

2. Analysis of acoustic process emission

The excerpt of the x-ray recordings in Fig. 16(a) shows that the process regime changes between deep penetration welding and heat conduction welding with the frequency that was set for beam oscillation in the z-direction. Those effects are also reflected in the audio signal in Fig. 16(b) especially in the first part of the process until 200 ms and around 400 ms. The experiment was also conducted with an active cross jet, which reflects the increased ambient noise in the spectrogram in Fig. 16(b). In the detailed view, it becomes obvious that the audio signal amplitude drops periodically every 6.6 ms. This can be used to determine whether a vapor capillary is present or not. Notably, the sample also shows a correlation between pore formation and corresponding inclusions in the base material [see Fig. 16(c)] but a comparatively low porosity in the other areas. The correlation of regime change and acoustic emission was also investigated in Ref. 28.

Correlation of the data shows that keyhole phenomena like a collapse of the capillary and piercing of cavities in aluminum die-cast welding can be detected. This enables, for instance, the filtering out of defective parts for a more detailed analysis, facilitating a well-informed decision regarding the rework of the component. Building on the insights gained, the data can be used in the future to train machine learning models.

V. CONCLUSION

The analysis of the x-ray investigations shows that aluminum die-castings are challenging materials in terms of their weldability because, in addition to the classic mechanisms of pore formation (e.g., gas solubility and keyhole phenomena) inclusions in the material like gas cavities or release agents can dramatically influence the process.

In the present study, different welding regime types were observed. Through dynamic beam oscillation, it is possible to significantly reduce pore formation and the creation of ejections. At high oscillation frequencies, this leads to an expansion of the vapor capillary and a change in the melt pool shape as well as its dynamics.

Both the differences between the regimes of locally oscillating keyhole and expanded capillary, as well as process irregularities such as spatters, can be detected in the audio signal. This provides a good basis for process monitoring and enables strategies for repair welding and process optimization.

The considerations of expanding the oscillation pattern in the z-direction show an initial approach for melt pool shaping and also reveal correlations between the audio signal and the keyhole formation. Further investigations are required in order to face the higher complexity of process parameter selection and the transfer to industrial applications.

ACKNOWLEDGMENTS

This work was supported by the Fraunhofer Internal Programs under Grant No. PREPARE 40-02931. We acknowledge the Paul Scherrer Institut, Villigen, Switzerland for provision of synchrotron radiation beamtime at the TOMCAT beamline X02DA of the SLS and would like to thank Christan M. Schlepütz, Tillmann R. Neu, and Philipp Mohlau for assistance.

AUTHOR DECLARATIONS

Conflict of Interest

The authors have no conflicts to disclose. In the writing process during the preparation of this work, the authors used "DeepL Write" and "FhGenie" in some places in order to improve language and readability. After using those tools, the authors reviewed and edited the content as necessary and they take full responsibility for the content of the publication.

Author Contributions

Stephan Börner: Conceptualization (lead); Data curation (equal); Formal analysis (lead); Investigation (lead); Methodology (equal); Visualization (lead); Writing – original draft (lead). **Dirk Dittrich:** Conceptualization (supporting); Funding acquisition (equal); Resources (lead). **Tim Sahm:** Data curation (equal); Investigation (equal); Visualization (equal); Writing – review & editing (equal). **Linda Ullmann:** Data curation (equal); Writing – review & editing (equal). **Paul Hans Kamm:** Investigation (equal); Methodology (equal); Writing – review & editing (equal). **Axel Jahn:** Conceptualization (supporting); Funding acquisition (equal); Resources (equal).

DATA AVAILABILITY

The data that support the findings of this study are available from the corresponding author upon reasonable request.

REFERENCES

[1]N. Seto, S. Katayama, and A. Matsunawa, "Porosity formation mechanism and suppression procedure in laser welding of aluminium alloys," Weld. Int. **15**, 191–202 (2001).
[2]W. Gref, "Laserstrahlschweißen von Aluminiumwerkstoffen mit der Fokusmatrixtechnik," Ph.D. thesis, University Stuttgart, Germany, 2005.
[3]M. Pastor, H. Zhao, and T. Debroy, "Pore formation during continuous wave Nd:YAG laser welding of aluminium for automotive applications," Weld. Int. **15**, 275–281 (2001).
[4]C. Hagenlocher, J. Lind, R. Weber, and T. Graf, "High-speed X-ray investigation of pore formation during full penetration laser beam welding of AA6016 aluminum sheets contaminated with lubricants," Appl. Sci. **10**, 2077 (2020).
[5]S. Börner, D. Dittrich, P. Mohlau *et al.*, "*In situ* observation with x-ray for tentative exploration of laser beam welding processes for aluminum-based alloys," J. Laser Appl. **33**, 012026 (2021).
[6]M. Hummel, C. Hagenlocher, A. Haeusler *et al.*, "Analysis on the influence of vapor capillary aspect ratio on pore formation in laser beam welding of aluminum," J. Mater. Process. Technol. **312**, 117862 (2023).
[7]F. Teichmann, S. Müller, and K. Dilger, "Investigations on dual laser beam welding of aluminum high pressure die-castings at reduced ambient pressure," J. Laser Appl. **30**, 032420 (2018).
[8]A. Fritzsche, K. Hilgenberg, F. Teichmann, H. Pries, K. Dilger, and M. Rethmeier, "Improved degassing in laser beam welding of aluminum die-casting by an electromagnetic field," J. Mater. Process. Technol. **253**, 51–56 (2018).
[9]S. Völkers, S. Böhm, and V. Somonov, "Porosity reduction in the laser beam welding of aluminium die-cast alloys through the overlapping of mechanically induced sound waves," J. Phys.: Conf. Ser. **1109**, 012019 (2018).
[10]R. Winkler, "Porenbildung beim Laserstrahlschweissen von Aluminium-Druckguss," Ph.D. thesis, University Stuttgart, Germany, 2003.
[11]S. Ulrich, M. Rosenblatt, and M. Pieper, "Herstellung Hybrider Komponenten Mittels Laserstrahl-Schweißen," in *Proceedings of Lasertagung, Mittweida, Germany, 10-11 November 2021* (Hochschule Mittweida, Mittweida, 2021)
[12]M. Möller, P. Haug, P. Scheible, C. Buse, C. Frischkorn, and N. Speker, "Spatially tailored laser energy distribution using innovative optics for gas-tight welding of casted and wrought aluminum alloys in e-mobility," J. Laser Appl. **34**, 042015 (2022).
[13]M. Sokolov, P. Franciosa, and D. Ceglarek, "Remote laser welding of die-casting aluminum parts for automotive applications with beam oscillation and adjustable ring mode laser," in *Proceedings of LiM, Munich, Germany, 21-24 June 2021* (German Scientific Laser Society, Munich, 2021).
[14]D. Dittrich, A. Jahn, J. Standfuss, and E. Beyer, "Laser beam welding of atmosphere aluminum die-cast material using high frequency beam oscillation and brilliant beam sources," J. Laser Appl. **29**, 022425 (2017).
[15]C. Schäfer, "Druckdichtes Schweißen von Aluminium-Druckgussbauteilen mittels Laserverfahren," ATZproduktion **7**, 44–47 (2020).
[16]E. Beyer, *Schweißen mit Laser* (Springer-Verlag, Berlin, 1995), p. 5.
[17]A. J. Birnesser, "Prozessregelung beim Laserstrahlschweißen," Ph.D. thesis, University Stuttgart, Germany, 2011.
[18]R. Olsson, I. Eriksson, J. Powell, A. V. Langtry, and A. F. H. Kaplan, "Challenges to the interpretation of the electromagnetic feedback from laser welding," Opt. Lasers Eng. **49**, 188–194 (2011).
[19]C. Mittelstädt, T. Mattulat, T. Seefeld, and M. Kogel-Hollacher, "Novel approach for weld depth determination using optical coherence tomography measurement in laser deep penetration welding of aluminum and steel," J. Laser Appl. **31**, 022007 (2019).
[20]J. Stavridis, A. Papacharalampopoulos, and P. Stavropoulos, "Quality assessment in laser welding: A critical review," Int. J. Adv. Manuf. Technol. **94**, 1825–1847 (2018).
[21]H. Luo, H. Zeng, L. Hu, X. Hu, and Z. Zhou, "Application of artificial neural network in laser welding defect diagnosis," J. Mater. Process. Technol. **170**, 403–411 (2005).
[22]A. Jahn, D. Dittrich, S. Börner *et al.*, "3-Dimensional beam shaping for dynamic adjustment of focus position and intensity distribution for laser welding and cutting," in *Proceedings of LiM, Munich, Germany, 21-24 June 2021* (German Scientific Laser Society, Munich, 2021).
[23]R. Mokso, C. M. Schlepütz, G. Theidel *et al.*, "GigaFRoST: The gigabit fast readout system for tomography," J. Synchrotron Radiat. **24**, 1250–1259 (2017).
[24]M. Bührer, M. Stampanoni, X. Rochet, F. Büchi, J. Eller, and F. Marone, "High-numerical-aperture macroscope optics for time-resolved experiments," J. Synchrotron Radiat. **26**, 1161–1172 (2019).

[25]D. Li, C. Slater, H. Cai, X. Hou, Y. Li, and Q. Wang, "Joining technologies for aluminium castings—A review," Coatings **13**, 958 (2023).
[26]S. Börner, D. Dittrich, J. Barrios Laranaga *et al.*, "Enhanced process understanding for laser welding of copper and aluminum alloys with dynamic beam oscillation," in *Proceedings of LiM, Munich, Germany, 26-29 June 2023* (German Scientific Laser Society, Munich, 2023).
[27]F. Fetzer, M. Sommer, R. Weber, J.-P. Weberpals, and T. Graf, "Reduction of pores by means of laser beam oscillation during remote welding of AlMgSi," Opt. Lasers Eng. **108**, 68–77 (2018).
[28]M. Hamidi Nasab, G. Masinelli, C. de Formanoir *et al.*, "Harmonizing sound and light: X-ray imaging unveils acoustic signatures of stochastic inter-regime instabilities during laser melting," Nat. Commun. **14**, 8008 (2023).